Nano Energy (2014) 10, 259–267

Available online at www.sciencedirect.com

ScienceDirect

journal homepage: www.elsevier.com/locate/nanoenergy

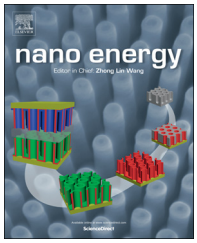

RAPID COMMUNICATION

Flexible silver grid/PEDOT:PSS hybrid electrodes for large area inverted polymer solar cells

Lin Mao[a], Qi Chen[a], Yaowen Li[a,c,*], Yang Li[a], Jinhua Cai[a], Wenming Su[b], Sai Bai[d], Yizheng Jin[d], Chang-Qi Ma[b], Zheng Cui[b], Liwei Chen[a,*]

[a]*Suzhou Institute of Nano-Tech and Nano-Bionics (SINANO), Chinese Academy of Sciences, Suzhou 215123, PR China*
[b]*Division of Printed Electronics, Suzhou Institute of Nano-Tech and Nano-Bionics (SINANO), Chinese Academy of Sciences, Suzhou 215123, PR China*
[c]*Jiangsu Key Laboratory of Advanced Functional Polymer Design and Application, Department of Polymer Science and Engineering, College of Chemistry, Chemical Engineering and Materials Science, Soochow University, Suzhou 215123, PR China*
[d]*State Key Laboratory of Silicon Materials, Department of Materials Science and Engineering, Zhejiang University, Hangzhou 310027, PR China*

KEYWORDS
Large area;
High efficiency organic solar cells;
Inverted solar cell;
Hybrid electrode;
Interfacial layer

Abstract
Bulk-heterojunction (BHJ) organic solar cell (OSC) has become a major thrust in solar energy research. It is highly critical to fabricate large-area high-efficiency OSCs in order to maximize the fraction of active area and hence their practical application. In this paper, we have fabricated a promising hybrid transparent electrode consisting of high resolution embedded silver grid (Ag-grid) in hybridization with high conductance poly(3,4-ethylenedioxythiophene):poly(styrenesulfonate) (PEDOT:PSS) (PH1000), which gives both high transparency and low sheet resistance. We further demonstrate its application in large-area high efficiency OSCs. By carefully tuning the properties of the Ag-grid based hybrid electrodes, the sheet resistance is further reduced to as low as 1.2 $\Omega\ sq^{-1}$. Inverted OSCs with device area of 1.21 cm^2 exhibited a record PCE of 3.36% for poly(3-hexylthiophene):[6,6]-phenyl-C_{61} butyric acid methyl ester (P3HT:$PC_{61}BM$) blend film as the active layer; and the PCE of PTB7:$PC_{71}BM$ devices reached 5.85%. To the best of our knowledge, the PCE of 5.85% is the highest in large-area flexible OSCs ($>1\ cm^2$) till date.

Introduction

Bulk-heterojunction (BHJ) organic solar cell (OSC) has become a major thrust in solar energy research [1–3]. Rapid progresses in materials development and device

*Corresponding authors.
E-mail addresses: ywli@suda.edu.cn (Y. Li), lwchen2008@sinano.ac.cn (L. Chen).

http://dx.doi.org/10.1016/j.nanoen.2014.09.007
2211-2855/

optimization have led to devices with power conversion efficiencies (PCEs) exceeding 10% [4,5], all these high-efficiency BHJ OSCs, however, are laboratory-scale devices with device areas typically no more than 0.1 cm^2. In practical applications, organic solar modules consist of active area, which are multiple OSCs connected in series and/or parallel, and inactive area such as wire, busbar and separator space. Therefore, it is highly critical to fabricate large-area high-efficiency OSCs in order to maximize the fraction of active area [6]. Once juxtaposing the reported PCEs with their corresponding device area (Supporting Information, Figure S1), we start to see a trend, in which only the so-called "small-area devices", i.e. devices with active area less than 1 cm^2 and usually prepared for the optimization of new materials and device configuration, show efficiency over 6% [7,8]. Whereas for any devices with area between 1 and 10 cm^2, or dubbed as "large-area devices" mostly used for the researches in modules of flexible solar cells, their efficiency could only reach the 3-4% range [9,10]. Furthermore, those "very-large devices" of greater-than-10 cm^2 area, which are investigated for large-scale production processes such as screen printing, shows their efficiency hovering at the range of merely 1-3% [11,12]. Such an anti-correlation between a PCE value and the corresponding device area is confirmed in systematic investigations on device area scaling [13], which reveals that reductions in short circuit current density (J_{sc}) and fill factor (FF) have led to a drastic lost in overall cell efficiency [14]. The deteriorated cell performance may arise from poor morphology related shorting paths and inefficient electron extraction [15], and/or significant increases in the series resistance of large-area cells due to the high sheet resistance of electrode materials ITO (10-15 $\Omega\,sq^{-1}$) [16]. In addition, ITO is mechanically brittle and thus is incompatible with the intended roll-to-roll manufacturing and flexible application of OSCs. The challenge of improving PCE for large area BHJ solar cells thus lies in constructing large-area transparent electrodes with ultra-low sheet resistance and establishing corresponding device fabrication processes for high quality film and desired device morphology.

We have recently reported a promising transparent electrode consisting of high resolution embedded silver grid (Ag-grid) in hybridization with high conductance poly(3,4-ethylenedioxythiophene):poly(styrenesulfonate) (PEDOT:PSS) (PH1000), which gives both high transparency and low sheet resistance of 4.5 $\Omega\,sq^{-1}$. Large area (1.21 cm^2) BHJ solar cells were obtained with a PCE of 1.36% [17]. In this paper, we further improve the Ag-grid based transparent electrode and demonstrate its application in large-area high efficiency OSCs. By carefully tuning the properties of the Ag-grid based hybrid electrodes, the sheet resistance is further reduced to as low as 1.2 $\Omega\,sq^{-1}$. Inverted OSCs with device area of 1.21 cm^2 exhibited a record PCE of 3.36% for poly(3-hexylthiophene):[6,6]-phenyl-C61 butyric acid methyl ester (P3HT:$PC_{61}BM$) blend film as the active layer; and the PCE of PTB7:$PC_{71}BM$ devices reached 5.85%. To the best of our knowledge, the PCE of 5.85% is the highest in large-area flexible OSCs (>1 cm^2) till date.

Moreover, we systematically investigated the factors limiting the PCE as the device area scales up using both ITO and Ag-grid cathodes. When ideal device morphology and contacts between layers are obtained, we found that the increase of cathode sheet resistance can account for the lost of PCE in scaling up to a great extent. Ag-grid cathodes are thus ideally suited for large-area device applications because of the ultra-low sheet resistance. Simulations show that the device PCE may remain at 3.80% when the device area is increased to 20.0 cm^2. Since the Ag-grid based hybrid electrode is compatible with mass production techniques such as roll-to-roll printing processes, our results demonstrate a possibility of turning laboratory-scaled devices into very large-area solar modules while keeping their high efficiency.

Results and discussion

Optical and conductivity properties of Ag-grid based electrode

The embedded Ag-grid used in this study is prepared by filling a high-resolution hexagonal pattern on flexible PET substrate with silver ink, similar to that in our previous report [17]. The Ag-grid on PET substrate shows an outstanding optical transparency (>85%) in the range between 400 and 800 nm, which covers the absorption window of most active materials (Figure 1a). The hybrid electrode PET/Ag-grid/PH1000 was then obtained by spin-coating PH1000 onto the PET/Ag-grid film. Smooth and pinhole-free films are prepared for PH1000 layer thicknesses between 80 nm and 200 nm (Figure S2). The sheet

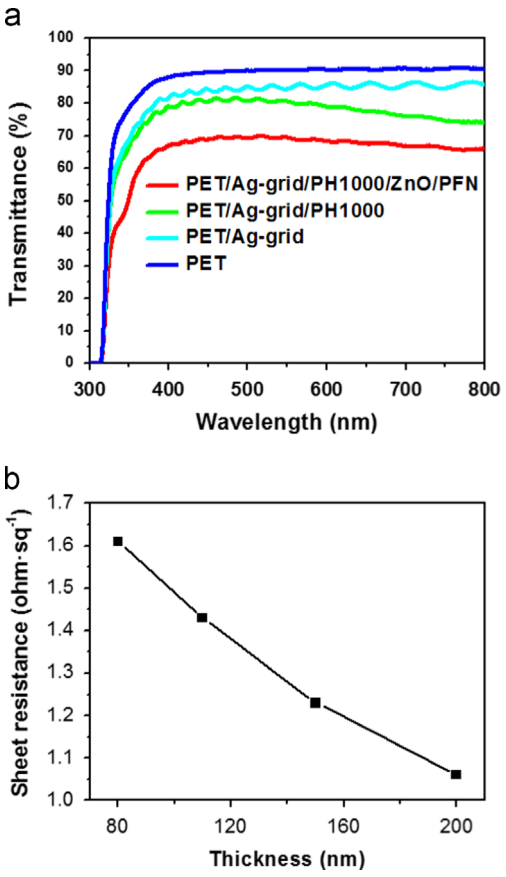

Figure 1 (a) Transmittance spectra of PET, PET/Ag-grid, PET/Ag-grid/PH1000 and PET/Ag-grid/PH1000/ZnO/PFN films; (b) Sheet resistances of PET/Ag-grid/PH1000 hybrid electrode with varied PH1000 thicknesses.

resistances of the hybrid electrode measured with a four-point probe shows a gradual decrease with increasing thickness of PH 1000 (Figure 1b). To balance the sheet resistance with the optical transparency, the PH1000 thickness was chosen to be 150 nm. The resulting hybrid electrode PET/Ag-grid/PH1000 shows an 80% transparency in the 400–800 nm range and an excellent sheet resistance of 1.2 ohm sq^{-1}, which is almost one order of magnitude lower than that of commercial ITO-glass substrates.

Further modification of the electrode with different interlayers is necessary for device applications. In the inverted BHJ OSC configuration, a ZnO layer is coated on the hybrid electrode to enhance electron extraction. The optical transparency in the visible range becomes ~70% after ZnO coating (Figure 1a), which is comparable to most other reported hybrid electrodes [18,19].

Fabrication and properties of organic solar cell

In order to demonstrate the application of the PET/Ag-grid/PH1000 electrode, inverted OSCs using P3HT or PTB7 as electron donors, and $PC_{61}BM$ or $PC_{71}BM$ as electron acceptors are prepared. The inverted device configuration can take advantage of vertical phase separation and the resulting concentration gradient in the active layer [20], and improve the device lifetime by using air-stable high work function metals as the top electrode [21,22]. ZnO nanoparticles and subsequent poly [(9,9-bis(3-(N,N-dimethylamino)propyl)-2,7-fluorene)-alt-2,7-(9,9-dioctylfluorene)] (PFN) layers are employed as the electron extraction layer. As shown in Figure 2a, the device stacking was PET/Ag-grid/PH1000/ZnO/PFN/active layer/MoO_3/Ag. Molecular structure of the active and interlayer materials is listed in Figure 2b; and the energy levels of these materials are depicted in Figure 2c. The conducting band minimum for ZnO is 4.4 eV below vacuum [23], which is close to the lowest unoccupied molecular orbital (LUMO) level of $PC_{61}BM$ and $PC_{71}BM$ (4.3 eV) [23,24]. The energy level matching suggests that ZnO can efficiently extract electrons from the active layer. Furthermore, a 10-nm-thin layer of PFN was applied on top of the ZnO layer to reengineer the interface between the ZnO electron extraction layer and the active layer, which reportedly can improve interfacial contact and enhance charge transport due to its interfacial electrical dipole [25,26]. A molybdenum oxide (MoO_3) thin film was selected as the hole extraction layer. The valence band maximum (VBM) of MoO_3 is 5.4 eV [27], which is close to the highest occupied molecular orbital (HOMO) of P3HT and PTB7. Thus, holes can be efficiently transported to the Ag anode without significant loss in energy.

A photograph of a 1.1×1.1 cm^2 flexible inverted device based on the PET/Ag-grid/PH1000 hybrid electrode is shown in the inset of Figure 3a. The current density–voltage (J–V) characteristics of the large-area devices under 100 mW/cm^2 AM 1.5 G illumination are shown in Figure 3a. The PTB7:$PC_{71}BM$ based devices show open circuit voltage (V_{oc}) of 0.7 V, J_{sc} of 13.72 mA/cm^2, FF of 0.61, and PCE of 5.85%, which are the highest values reported so far for OSCs with device area greater than 1.0 cm^2. Meanwhile, the P3HT:$PC_{61}BM$ based devices also show a relatively high PCE of 3.36%, which is comparable with that of glass/ITO electrode based device. The corresponding

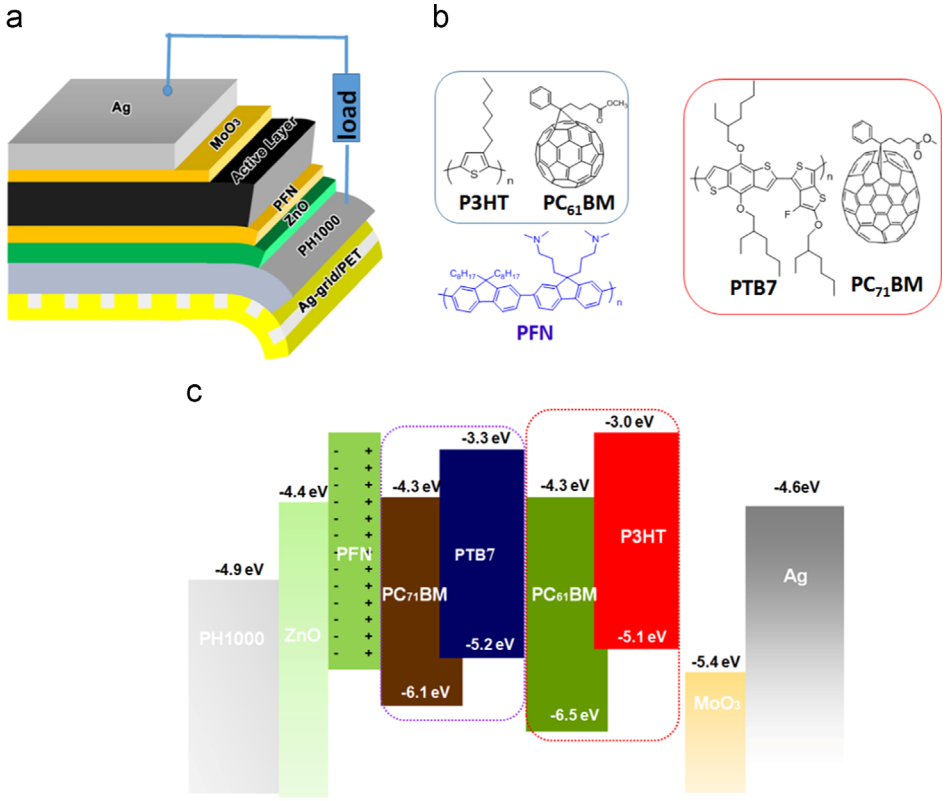

Figure 2 (a) The device structure of the flexible inverted solar cell; (b) the molecular structures of the active layer components and the interfacial layers; (c) energy level diagram of the materials used in the devices.

photovoltaic performance parameters are extracted and summarized in Table 1. Control devices with the hybrid electrode in the conventional device stacking PET/Ag-grid/PH1000/PEDOS:PSS-4083/active layer/LiF/Al are also prepared and their device parameters also included in Table 1 for comparison. It is clear that the PET/Ag-grid/PH1000 electrode based inverted OSCs show significantly better photovoltaic performances, especially in J_{sc} and FF, than conventional configuration devices for both P3HT:PC_{61}BM and PTB7:PC_{71}BM active layers. The ZnO/PFN interlayer may benefit the electron collection efficiency via suppressing bimolecular recombination and facilitating electron transport [25]. The improved J_{sc} and FF are fully consistent with the smaller series resistance (R_s) and greater shunt resistance (R_{sh}) of inverted OSCs compared to those of corresponding conventional OSCs (Table 1).

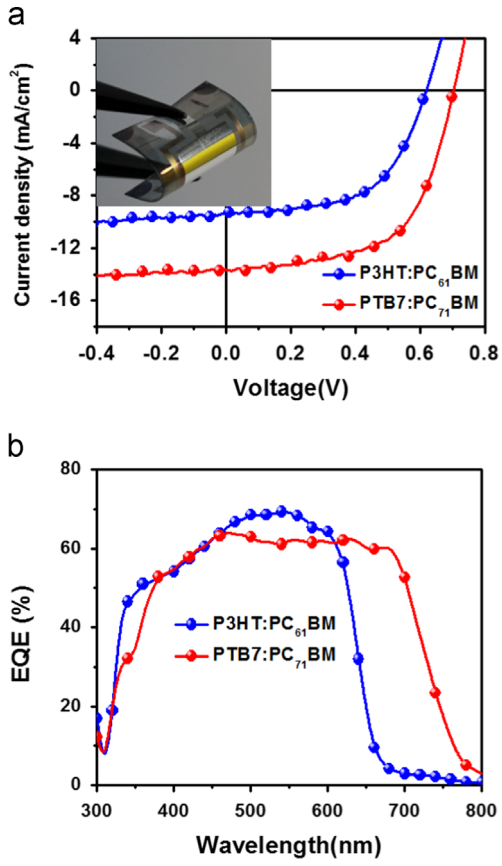

Figure 3 Inverted OSCs based on PET/Ag-grid/PH1000/ZnO/PFN/Active layer/MoO_3/Ag device configuration with device area 1.21 cm^2 (a) *J-V* characteristics for active layer P3HT:PC_{61}BM and PTB7:PC_{71}BM under AM 1.5 G, 100 mW/cm^2 white light illumination. Inset of (a) shows the photograph of PET/Ag-grid/PH1000-based flexible inverted OSCs; (b) EQE spectra for active layer P3HT:PC_{61}BM and PTB7:PC_{71}BM.

Figure 3b shows the external quantum efficiency (EQE) spectra of the inverted OSCs. The inverted OSCs for active layers P3HT:PC_{61}BM and PTB7:PC_{71}BM show strong and broad response from 320 nm to 660 nm, and 320 nm to 780 nm, respectively. Meanwhile, the J_{sc} values calculated from the integral of EQE curves with an AM 1.5 G reference spectrum are consistent with that obtained from the *J-V* measurement. All these indicate that the hybrid electrode in combination with the inverted device configuration lead to efficient photoresponse for various photoactive layer.

An important factor that may notably affect the device performance is the device morphology. In order to analyze the effect of morphology on the device performance, the topography of the PH1000, ZnO and PTB7:PC_{71}BM films were investigated by atomic force microscopy (AFM) and cross-sectional scanning electron micrographs (SEM). As shown in Figure 4a-c, large-area uniform PH1000, ZnO and PTB7:PC_{71}BM films on the Ag-grid substrates are observed. The root mean square (RMS) roughness values are 1.4 nm, 3.5 nm, and 3.8 nm, respectively, which indicates that the Ag-grid groove may slightly influence the quality of spin-coated films. Interestingly, spin-coated ZnO nanoparticle layer is observed to smooth the Ag-grid grooves and even the edge roughness of the grooves (Figure S3). Furthermore, the reengineered interface layer ZnO/PFN also greatly improves the surface wettability for subsequent active layers and results in a tightly stacked multilayer composite film, which is clearly evidenced from the cross-sectional electron micrographs of the device in Figure 4d and e. Compared to our previously reported morphology of PET/Ag-grid/PH1000 electrode-based devices with the conventional device configuration [17], the inverted devices show continuous and smooth surface features as well as good adhesion between contacting layers. Such morphological improvement may significantly enhance electrical contact and reduce the probability of microscopic shorting such as pinholes. These effects are manifested in the low series resistance R_s and high shunt resistance R_{sh}, and hence the high FF and J_{sc} in inverted OSCs.

A critical factor that gives rise to the high performance of the inverted OSC is the low sheet resistance of the large-area cathode. In order to understand the origin of the excellent performance, various control devices with different device area and cathode materials were also fabricated under similar conditions. All the photovoltaic performance

Table 1 Performance of PET/Ag-grid/PH1000 electrode based OSCs with varied device configurations and active layers.

Device area (cm^2)	Bottom electrode	*Active layer*	V_{oc} (V)	J_{sc} (mA/cm^2)	*FF*	PCE (%)	R_s (Ω cm^2)	R_{sh} (KΩ cm^2)
1.21	PET/Ag-grid/PH1000[a]	P3HT:PC_{61}BM	0.61	7.91	0.52	2.52	9.3	9.0
1.21	PET/Ag-grid/PH1000 [b]	P3HT:PC_{61}BM	0.62	9.5	0.57	3.36	6.2	15.4
1.21	PET/Ag-grid/PH1000 [a]	PTB7:PC_{71}BM	0.66	12.1	0.47	3.75	7.2	4.1
1.21	PET/Ag-grid/PH1000[b]	PTB7:PC_{71}BM	0.7	13.7	0.61	5.85	4.7	6.3

[a]Conventional device configuration PET/Ag-grid/PH1000/PEDOS:PSS-4083/active layer/LiF/Al.
[b]Inverted device configuration PET/Ag-grid/PH1000/ZnO/PFN/active layer/MoO_3/Ag.

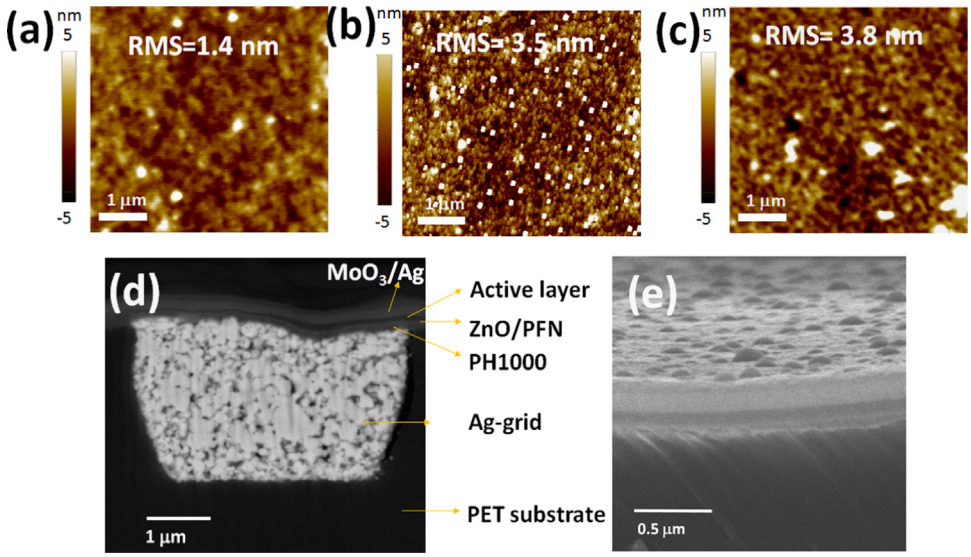

Figure 4 AFM images of (a) PH1000 film on PET/Ag-grid substrate; (b) ZnO film on PET/Ag-grid/PH1000 substrate; (c) active layer on PET/Ag-grid/PH1000/ZnO/PFN substrate. Cross-sectional SEM images of inverted OSCs based on large-area Ag-grid based hybrid electrode; (d) an area above a Ag-grid line; (e) an area between Ag-grid lines.

Table 2 Performance of inverted OSCs with varied substrates, device areas and active layers.

Device area (cm^2)	Bottom electrode	*Active layer*	V_{oc} (V)	J_{sc} (mA/cm^2)	*FF*	PCE (%)	R_s (Ω cm^2)	R_{sh} (KΩ cm^2)
1.0	PET/Ag-grid/PH1000	PTB7:$PC_{71}BM$	0.7	13.7	0.59	5.67	2.4	31.4
1.0	Glass/ITO	PTB7:$PC_{71}BM$	0.72	11.9	0.47	4.06	13.2	50.0
0.36	PET/Ag-grid/PH1000	PTB7:$PC_{71}BM$	0.7	13.8	0.6	5.80	1.2	63.7
0.36	Glass/ITO	PTB7:$PC_{71}BM$	0.72	13.5	0.55	5.38	5.1	6.7
0.09	PET/Ag-grid/PH1000	PTB7:$PC_{71}BM$	0.72	13.9	0.6	6.01	0.5	22.7
0.09	Glass/ITO	PTB7:$PC_{71}BM$	0.71	16.2	0.61	7.02	1.2	13.7

parameters were extracted and summarized in Table 2. Figure 5a and b shows representative *J-V* characteristics of inverted OSCs with varied device areas (0.09 cm^2, 0.36 cm^2, 1.0 cm^2) in PET/Ag-grid/PH1000/ZnO/PFN/PTB7:$PC_{71}BM$/MoO_3/Ag device stacking along with those of the control devices with the same stacking but on glass/ITO electrodes. The average values of R_s and R_{sh}, which are estimated by fitting the dark *J-V* curves with the Shockley diode equation, are included in Table 2. Although PET/Ag-grid/PH1000-based OSCs exhibited inferior performances than glass/ITO-based cells in small-area devices, they have much better device area scaling behavior and show superior performances in large-area devices. For example, a glass/ITO-based inverted OSC with device area 0.09 cm^2 exhibited a J_{sc} of 16.2 mA/cm^2, a V_{oc} of 0.71 V, and a FF of 0.61, resulting in a PCE of 7.02%. Meanwhile, PET/Ag-grid/PH1000-based inverted OSC with device area 0.09 cm^2 had a reasonably high PCE of 6.01% (J_{sc}=13.9 mA/cm^2, V_{oc}=0.72 V, FF=0.60). The major cause of the slightly lower PCE of PET/Ag-grid/PH1000-based inverted OSCs is the decrease in their J_{sc} value, which is due to the reduction in optical transparency of the PET/Ag-grid/PH1000/ZnO substrate in the visible region (Figure 1a). Importantly, as the device area increase from 0.09 cm^2, 0.36 cm^2 to 1.0 cm^2, the PET/Ag-grid/PH1000-based inverted OSCs exhibit little deterioration in photovoltaic performances. Even in the 1.21 cm^2 cell, a high PCE of 5.85% can be still obtained. On the other hand, the glass/ITO-based inverted OSCs show significantly decreased J_{sc} and FF when device area scales up. The J_{sc} and FF of the 1.0 cm^2 cell are more than 26% and 22% lower than that of the 0.09 cm^2 cell, respectively.

To better understand this phenomenon, the evolution of the corresponding parameters with device area is displayed in Figure 5c-e. It shows that V_{oc}, which is related to the donor/acceptor junction properties and/or the work function difference between the cathode and anode [28,29], only changes slightly with cell area for both ITO and Ag-grid electrodes. On the other hand J_{sc} and FF, which are significantly affected by R_s, show significant device area dependence, especially in glass/ITO-based cells. In this device configuration, the R_s can be expressed as the following:

$$R_s = (1/a)SR_{sheet} + (r_{ZnO}t_{ZnO} + r_{active}t_{active} + r_{MoO_3}t_{MoO_3}) \quad (1)$$

in which S is the active area of device, R_{sheet} is the sheet resistance of bottom electrode, r and t refer to the

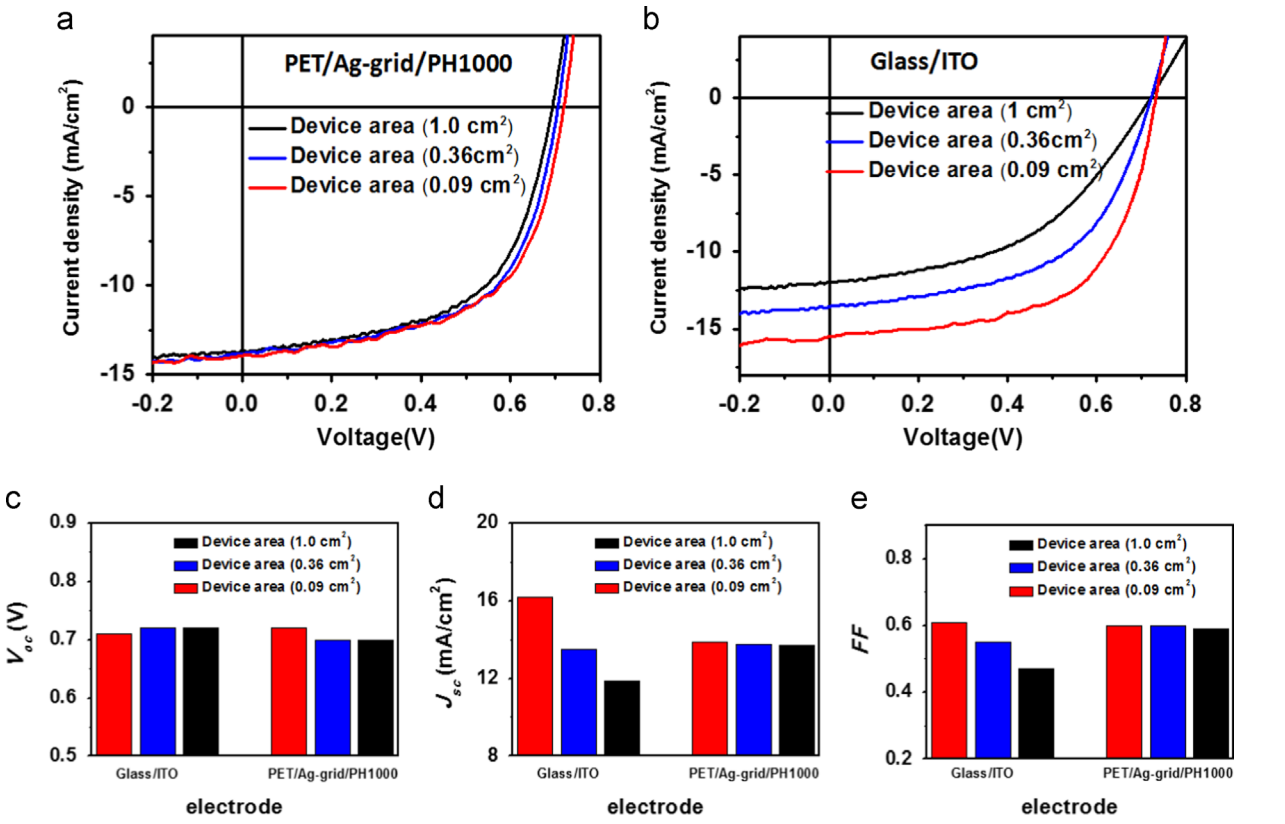

Figure 5 *J-V* characteristics of inverted OSCs fabricated with PTB7:$PC_{71}BM$ with different device areas under AM 1.5G white light illumination (a) based on the PET/Ag-grid/PH1000 electrode; (b) based on Glass/ITO electrode. The evolution of (c) V_{oc}, (d) J_{sc} and (e) *FF* for different device areas.

resistivity and thickness of different layers, respectively; *a* is a constant related with the measurement geometry [14]. Linear fits of R_s (PTB7:$PC_{71}BM$ based devices) against device area for both Ag-grid and ITO electrodes are presented in Figure 6a. The two fittings show almost identical intercepts of 0.2 and 0.3 $\Omega\,cm^2$, but significantly different slopes of 13.1 and 2.1 Ω for the glass/ITO and Ag-grid hybrid electrodes, respectively. Qualitatively, this agrees well with the Eq. (1) that the intercept is not dependent on cell area, and the slope is directly proportional to the sheet resistance, which almost differ by an order of magnitude for ITO and Ag-grid hybrid electrodes. Quantitatively, the slope of the fittings for ITO and Ag-grid hybrid electrode based devices is almost equal to the sheet resistance of the two electrode materials, i.e. 14.1 and 1.2 $\Omega\,sq^{-1}$, respectively. This indicates that the effect of cathode sheet resistance can largely account for the lost of PCE in device area scaling. Ag-grid hybrid electrodes are thus ideally suited for large-area device applications because of the ultra-low sheet resistance (1.2 $\Omega\,sq^{-1}$).

In order to further evaluate the potential of PET/Ag-grid/PH1000 in very large area OSCs (active area $>10\,cm^2$), the Shockley diode equation based on an equivalent circuit model, is used to simulate the *J-V* characteristics [30,31]:

$$J = J_0\left\{\exp\left(\frac{V-JR_s}{nkt/e}\right)-1\right\}+\frac{V-JR_s}{R_{sh}}-J_{ph} \quad (2)$$

where *k* is the Boltzmann constant, *T* is the temperature, *e* is the elementary charge, *n* is the ideality factor, J_0 is reverse saturation current density, J_{ph} is photocurrent density generated when the solar cell is illuminated. Figure 6b shows the simulated *J-V* curves of Ag-grid based inverted devices with the PTB7:$PC_{71}BM$ active material as the device area further scales up. Parameters used in the simulation such as J_0=0.001 mA/cm^2, n=2.5, R_{sh}=10,000 $\Omega\,cm^2$, J_{ph}=13.6 mA/cm^2 are obtained from the fitting of the experimental measured data of the 1.0 cm^2 device (Figure 5a), except for the R_s, which are obtained from the Eq. (1) using the fitted slope and intercept parameters for the PET/Ag-grid/PH1000 electrode as in Figure 6a. The results show that V_{oc} does not change with increased device area; FF is significantly reduced as the device area increases; and J_{sc} remains relatively stable and seriously decreases only at very large device area. It is exciting that there is no significant deterioration in PCE until the device area is as large as 10.0 cm^2. Even when the area-scaling is scaled up to 20.0 cm^2, the PCE still retain 60% of the small-area device value. This suggests that with the Ag-grid based hybrid electrode and the inverted device configuration, the cells can be scaled up to 10.0 cm^2 without too much compromise in its performance. Considering the compatibility of the flexible electrode with mass production techniques such as roll-to-roll printing, these results provide an important approach towards large-scale production of OSCs.

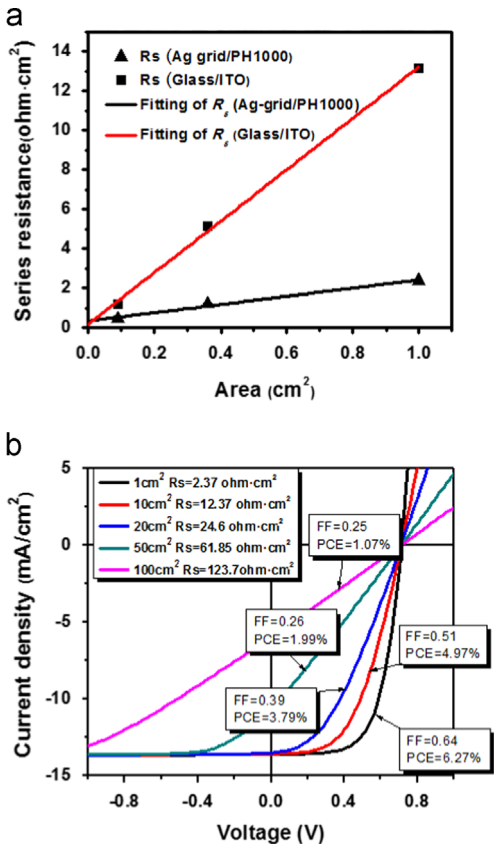

Figure 6 (a) Device series resistances versus active areas. Solid lines represent linear fits of the data; (b) simulation of *J-V* curves with various device area based on Ag-grid/PH1000 electrode and PTB7:$PC_{71}BM$ active layer.

Conclusion

Large-area flexible OSCs were prepared using PET/Ag-grid/PH1000 hybrid electrodes. High PCE of 3.36% and 5.85% were obtained for 1.21 cm^2 area inverted devices with P3HT:$PC_{61}BM$ and PTB7:PC71BM active materials, respectively. The improved performance of the large area devices is attributed to the low sheet resistance of the PET/Ag-grid/PH1000 hybrid electrode and the smooth surface morphology partially due to the ZnO/PFN electron extraction layer. Detailed *J-V* characteristics fitting of PET/Ag-grid/PH1000 and glass/ITO electrodes based devices with different active area indicates that the increased series resistance R_s is the major cause of efficiency lose in large-area devices. R_s scales linearly with active device area and the slope is controlled by the sheet resistance of the electrode material. Extrapolation of R_s to very large device area predicts that the PCE of PET/Ag-grid/PH1000 electrode based OSCs may remain at 3.8% even when the device area reaches 20 cm^2. These results highlight that reducing the sheet resistance of the transparent electrode is vitally important towards high efficiency OSCs on practical scales. The high-resolution embedded silver grid based hybrid electrode developed in this study not only exhibits ultra-low sheet resistance but also is compatible with large area roll-to-roll production, and thus it is highly promising for practical application of OSCs.

Experimental section

Fabrication of OSCs

PH1000 (Heraeus, Clevios PH1000, Germany) solution was first spin-coated at 600 rpm on the PET/Ag-grid after passing through a 0.45 μm filter and then baked at 120 °C for 30 min in air, resulting in a dry layer of 150 nm thick. A 35 nm thick buffer layer of PEDOT:PSS (Heraeus, Clevios PVPAI 4083, Germany) was subsequently spin-coated at 3500 rpm and baked at 120 °C for 15 min in air for the conventional device stacking. For the inverted device configuration, ZnO film (30 nm) and PFN (10 nm) were then coated on the hybrid electrode. ZnO nanoparticles was prepared by literature methods [32] and PFN were synthesized according to the reported methods [33]. The P3HT (Organic Nano Electronic material, Canada) and $PC_{61}BM$ (American Dye Source, Canada) blend film was prepared by dissolving in 1,2-dichlorobenzene (1 ml) a mixture of P3HT:$PC_{61}BM$ (20 mg:16 mg), then spin-coating at 600 rpm for 1 min and thermal annealing at 110 °C for 10 min under N_2. In the case of PTB7:$PC_{71}BM$ based device, PTB7 (8 mg) (Organic Nano Electronic material, Canada) and $PC_{71}BM$ (12 mg) (American Dye Source, Canada) were dissolved in a mixed solvent of chlorobenzene/1,8-diiodoctane (1 ml, 97:3% by volume) and spin-coated at 1000 rpm for 1 min to form an active layer with thickness of 90 nm. Then, the samples were then loaded into a vacuum chamber (4×10^{-4} Pa) for thermal evaporation of the top electrode. For the conventional devices, a layer of LiF (0.7 nm) and a layer of Al (100 nm) were deposited. For the inverted device, a layer of MoO_3 (10 nm) and a layer of Al (100 nm) were deposited. The effective photovoltaic area was defined by the geometrical overlap between the bottom anode and the top cathode.

Characterization

J-V characteristics of the solar cells were obtained using a Keithley 2635A source meter in the dark and under illumination of 100 mW/cm^2 white light from a Hg-Xe lamp filtered by a Newport 81094 Air Mass Filter. The illumination intensity was calibrated by a reference cell (Newport, Oriel 91150V, United States). The external quantum efficiency measurement system (Newport, Oriel IQE-200, United States) was used to determine the EQE spectra. The *J-V* and EQE measurements were performed under ambient atmosphere at room temperature. AFM image and the film thickness measurements were carried out on an Agilent 5500 atomic force microscope. The cross-section samples were prepared by Gatan Ilion and characterized using FEI Quanta 400 FEG Scanning Electron Microscope. The transmittance spectra were taken using a Perkin-Elmer Lambda 950 spectrophotometer. The sheet resistances were measured by Four-Point-Probing System (Bridge Technology, RM3000, United States).

Acknowledgments

This work was supported by the National Natural Science Foundation of China (Nos.: 91233104, 21204057 and 51172203), and the National Basic Research Programof China (2010CB934700). L.C. acknowledges the support from Jiangsu Provincial Natural Science Foundation (Grant no. BK20130006). The work at Soochow University was supported by Jiangsu Provincial Natural Science Foundation (Grant no. BK2012213).

Appendix A. Supporting information

Supplementary data associated with this article can be found in the online version at http://dx.doi.org/10.1016/j.nanoen.2014.09.007.

References

[1] B. Winther-Jensen, F.C. Krebs, Sol. Energy Mater. Sol. Cells 90 (2006) 123–132.
[2] C. Lungenschmied, G. Dennler, H. Neugebauer, S.N. Sariciftci, M. Glatthaar, T. Meyer, A. Meyer, Sol. Energy Mater. Sol. Cells 91 (2007) 379–384.
[3] G. Li, R. Zhu, Y. Yang, Nat. Photon. 6 (2012) 153–161.
[4] W. Li, A. Furlan, K.H. Hendriks, M.M. Wienk, R.A.J. Janssen, J. Am. Chem. Soc. 135 (2013) 5529–5532.
[5] J. You, L. Dou, K. Yoshimura, T. Kato, K. Ohya, T. Moriarty, K. Emery, C.-C. Chen, J. Gao, G. Li, Y. Yang, Nat. Commun. 4 (2013) 1446.
[6] F.C. Krebs, T. Tromholt, M. Jorgensen, Nanoscale 2 (2010) 873–886.
[7] S.J. Lou, J.M. Szarko, T. Xu, L. Yu, T.J. Marks, L.X. Chen, J. Am. Chem. Soc. 133 (2011) 20661–20663.
[8] Y. Liang, Z. Xu, J. Xia, S.-T. Tsai, Y. Wu, G. Li, C. Ray, L. Yu, Adv. Mater. 22 (2010) E135–E138.
[9] H. Jin, C. Tao, M. Velusamy, M. Aljada, Y. Zhang, M. Hambsch, P.L. Burn, P. Meredith, Adv. Mater. 24 (2012) 2572–2577.
[10] W. Kylberg, F.A. de Castro, P. Chabrecek, U. Sonderegger, B.T.-T. Chu, F. Nüesch, R. Hany, Adv. Mater. 23 (2011) 1015–1019.
[11] F.C. Krebs, J. Fyenbo, M. Jorgensen, J. Mater. Chem. 20 (2010) 8994–9001.
[12] B. Zimmermann, H.F. Schleiermacher, M. Niggemann, U. Würfel, Sol. Energy Mater. Sol. Cells 95 (2011) 1587–1589.
[13] S.-Y. Park, W.-I. Jeong, D.-G. Kim, J.-K. Kim, D.C. Lim, J.H. Kim, J.-J. Kim, J.-W. Kang, Appl. Phys. Lett. 96 (2010) 173301.
[14] A.J. Das, K.S. Narayan, Adv. Mater. 25 (2013) 2193–2199.
[15] W. Gaynor, G.F. Burkhard, M.D. McGehee, P. Peumans, Adv. Mater. 23 (2011) 2905.
[16] W.-I. Jeong, J. Lee, S.-Y. Park, J.-W. Kang, J.-J. Kim, Adv. Funct. Mater. 21 (2011) 343–347.
[17] Y. Li, L. Mao, Y. Gao, P. Zhang, C. Li, C. Ma, Y. Tu, Z. Cui, L. Chen, Sol. Energy Mater. Sol. Cells 113 (2013) 85–89.
[18] Y. Galagan, J. Rubingh, R. Andriessen, C. Fan, P. Blom, S. Veenstra, J.M. Kroon, Sol. Energy Mater. Sol. Cells 95 (2011) 1339–1343.
[19] J.-S. Yu, I. Kim, J.-S. Kim, J. Jo, T.T. Larsen-Olsen, R.R. Sondergaard, M. Hosel, D. Angmo, M. Jorgensen, F.C. Krebs, Nanoscale 4 (2012) 6032–6040.
[20] Z. Xu, L.-M. Chen, G. Yang, C.-H. Huang, J. Hou, Y. Wu, G. Li, C.-S. Hsu, Y. Yang, Adv. Funct. Mater. 19 (2009) 1227–1234.
[21] C.-H. Hsieh, Y.-J. Cheng, P.-J. Li, C.-H. Chen, M. Dubosc, R.-M. Liang, C.-S. Hsu, J. Am. Chem. Soc. 132 (2010) 4887–4893.
[22] J. Huang, G. Li, Y. Yang, Adv. Mater. 20 (2008) 415–419.
[23] Y. Sun, J.H. Seo, C.J. Takacs, J. Seifter, A.J. Heeger, Adv. Mater. 23 (2011) 1679–1683.
[24] Y. Li, L. Xue, H. Li, Z. Li, B. Xu, S. Wen, W. Tian, Macromolecules 42 (2009) 4491–4499.
[25] T. Yang, M. Wang, C. Duan, X. Hu, L. Huang, J. Peng, F. Huang, X. Gong, Energy Environ. Sci. 5 (2012) 8208–8214.
[26] Z. He, C. Zhong, X. Huang, W.-Y. Wong, H. Wu, L. Chen, S. Su, Y. Cao, Adv. Mater. 23 (2011) 4636–4643.
[27] Z. He, C. Zhong, S. Su, M. Xu, H. Wu, Y. Cao, Nat. Photon. 6 (2012) 591–595.
[28] D. Cheyns, J. Poortmans, P. Heremans, C. Deibel, S. Verlaak, B.P. Rand, J. Genoe, Phys. Rev. B 77 (2008) 165332.
[29] C.J. Brabec, A. Cravino, D. Meissner, N.S. Sariciftci, T. Fromherz, M.T. Rispens, L. Sanchez, J.C. Hummelen, Adv. Funct. Mater. 11 (2001) 374–380.
[30] J.D. Servaites, S. Yeganeh, T.J. Marks, M.A. Ratner, Adv. Funct. Mater. 20 (2010) 97–104.
[31] S. Choi, W.J. Potscavage, B. Kippelen, J. Appl. Phys. 106 (2009) 054507.
[32] B. Sun, H. Sirringhaus, Nano Lett. 5 (2005) 2408–2413.
[33] F. Huang, H. Wu, D. Wang, W. Yang, Y. Cao, Chem. Mater. 16 (2004) 708–716.

Lin Mao is a Ph.D. candidate in National Laboratory for Optoelectronics in Wuhan, PR China. He acquired most of his scientific findings in SINANO (PR China) and received M.S. degree in USTC earlier 2014. Lin Mao is currently interested in flexible/large area organic electronics and NIR photodetection.

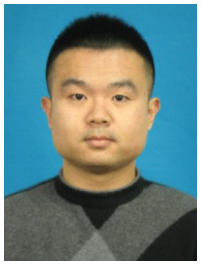

Qi Chen received his B.S. degree in physics from Zhengzhou University, China, in 2008 and Ph.D. degree in physics from University of Science and Technology of Chinain 2014. Heiscurrentlya postdoctoral researcherat-Suzhou Institute of Nano-Tech and Nano-Bionics, Chinese Academy of Sciences. His-research focuses on the investigation of interface properties of nanostructure opto-electronic devices by atomic force microscopy.

Yaowen Li received his Bachelor's Degree in the Departmentof Chemistry from Jilin University in 2005. He obtained his Ph.D. degreein the Department of Chemistry from Jilin University in 2010 under the supervision of Professor WenjingTian. Then he joined the College of Chemistry, Chemical Engineering and Materials Scienceof Soochow University, PR China, in 2010. He is currently anassociate professor of Soochow University. In the period from 2011 to 2014, he collaborated with Professor Liwei Chen as a postdoctor. Hisresearch focuses ondesign and synthesis of organic/polymer semiconductor, construction of supramolecular self-assembly ordered film, photovoltaic device fabrication and flexible large area solar cell.

Yang Li received his B.S. degree from Hubei University in 2011. He is currently a M.S. student in University of Science and Technology of China. His current research interests include organic solar cells and nanoimprint lithography.

Jinhua Cai received his B.Sc. and Ph.D. degrees in condensed matter physics from Nanjing University, China, in 1994 and 1999, respectively. He worked at the department of physics, Shanghai Jiao Tong University from 1999 to 2013 as postdoctoral researcher and associate professor. He is currently an associate professor at Suzhou Institute of Nano-tech and Nano-Bionics (SINANO), CAS. Hisresearch is currently focused on photovoltaic material and device physics.

Wenming Su received his Ph.D. degree from Changchun Institute of Optics, Fine Mechanics and Physics, Chinese Academy of Sciences, in 2007. He is currently an Associate professor in Printable Electronics Research Center, Suzhou Institute of Nano-tech, CAS. His research interests include OLED materials and device physics, metal mesh conductive transparent film, and flexible thin film encapsulation for organic & printed electronics.

Sai Bai received his Ph.D. degree in Materials Physics and Chemistry from Department of Material Science and Engineering, Zhejiang University, China in 2014. He is currently a postdoctoral fellow in the Solar and Photovoltaics Engineering Research Center at King Abdullah University of Science and Technology. His research interests focuses on the fabrication of low temperature solution processed metal oxide films (Sol-gel precursors and colloidal nanocrystal) and their applications on solution processed photovoltaic cells, light emitting diodes.

Yizheng Jin received a Ph.D. in Chemistry from University of Sussex, UK in 2005. After a 6-months stay in University of Surrey, he joined the OE group at Cavendish Lab, University of Cambridge. He is currently an associate professor at the School of Material Science and Engineering, Zhejiang University, China. His current research interests include solution-processed optoelectronic devices and material chemistry of oxide films.

Chang-Qi Ma received his bachelor's degree in Chemistry from Beijing Normal University in 1998. In 2003 he obtained his Ph.D. degree at the Technical Institute of Physics and Chemistry, Chinese Academy of Sciences in Beijing with Professor B.-W. Zhang. After that he was a postdoctoral research assistant at Heriot-Watt University in Edinburgh, UK with Dr. Graeme Cooke, until he joined the research group of Professor P. Bäuerle at the University of Ulm in 2004 as a Humboldt research fellow. From January 2007 till May 2011, he was doing his Habilitation at Institute of Organic Chemistry II and Advanced Materials, Ulm University. Since June 2011 he was appointed as a professor of chemistry at Suzhou Institute of Nano-Tech and Nano-Bionics, Chinese Academy of Sciences, China. His research interests mainly focus on solution processable photovoltaic technologies, especially in organic semiconductor based solar cells.

Zheng Cui is the Director of Printable Electronics Research Center at the Suzhou Institute of Nanotech, Chinese Academy of Sciences. He had his Ph.D. in Electronics Engineering in 1988 and from 1989 to 2009 worked at the Microelectronics Research Center of Cambridge University and Rutherford Appleton Laboratory in the UK. In 2009, after working 20 years in the UK, he returned to China and set up the first printed electronics research center at Suzhou Institute of Nanotech. He has published over 220 scientific papers and 6 monographs in the areas of micro/nanofabrication technologies and printed electronics. He led the R&D of transparent conductive film based on printed silver grids technology which is now manufactured in high volume to replace ITO for touch panels.

Liwei Chen got a B.S. from Department of Materials Science and Engineering, University of Science and Technology of China in 1993, a M.S. from School of Chemistry and Molecular Engineering, Beijing University in 1996, and Ph.D. from Department of Chemistry and Chemical Biology at Harvard University in 2001. After a “bridging” postdoc between Columbia University and IBM T.J. Watson Research Center, he started independent research as an assistant professor at the Department of Chemistry and Biochemistry at Ohio University in 2004. He moved to Suzhou Institute of Nano-tech and Nano-bionics (SINANO), Chinese Academy of Sciences in 2009. He is currently a professor of chemistry and serves as the Vice-director Research of SINANO. His research focuses on energy nanotechnology including thin-film solar cells and lithium batteries. As an expert in scanning probe microscopy, his approach integrates surface and interface analysis with materials development towards practical applications.